Dalton Transactions

ROYAL SOCIETY OF CHEMISTRY

PAPER

View Article Online
View Journal | View Issue

Check for updates

Cite this: *Dalton Trans.*, 2021, **50**, 9735

Electronic and magnetic states of Fe ions in Co_2FeBO_5†

Yurii V. Knyazev,[a] Natalia V. Kazak, *[a] Vyacheslav S. Zhandun, [a] Juan Bartolomé,[b] Ana Arauzo, [b,c] Nadejda A. Belskaya,[d] Oleg A. Bayukov,[a] Leonard N. Bezmaternykh‡[a] and Sergey G. Ovchinnikov[a]

Received 13th January 2021,
Accepted 12th May 2021

DOI: 10.1039/d1dt00125f

rsc.li/dalton

The ludwigite Co_2FeBO_5 has been studied experimentally using ^{57}Fe Mössbauer spectroscopy and theoretically using DFT + GGA calculations. The room-temperature Mössbauer spectra are composed of four quadrupole doublets corresponding to the high-spin Fe^{3+} ions in octahedral oxygen coordination. All components undergo splitting below 117 K due to the magnetic hyperfine fields. The DFT + GGA calculations performed for three models of Fe ion distributions have revealed that the ground state corresponds to the "Fe4(HS)" model with the high-spin Fe^{3+} ions located at the M4 site and the high-spin Co^{2+} ions located at the M1, M2, and M3 sites. A ferrimagnetic ground state, with the Co and Fe magnetic moments being nearly parallel to the *b*-axis and a total magnetic moment of *circa* 1.1μ_B f.u.$^{-1}$, was found. The other Fe distributions cause an increase in the local octahedral distortions and transformation of the spin state. The calculated quadrupole splitting values are in good agreement with the experimental values obtained by Mössbauer spectroscopy.

1. Introduction

Ferrimagnetic materials are considered as a platform for realizing fast device operation.[1,2] Unlike antiferromagnets, their magnetic states can be detected and manipulated by the applied magnetic fields or even by a single femtosecond laser pulse near the compensation and magnetic transition points.[3] In the former case, the magnetization reversal is achieved by domain-wall motion, while in the latter case by femtosecond laser pulse heating that acts as an instantaneously applied magnetic field. It has recently been demonstrated that the amorphous rare-earth (RE) transition-metal (TM) alloys, such as GdFeCo, demonstrate substantially different dynamics under optical excitation.[3,4] Most of the traditional ferrimagnets are multi-component systems in which the RE and TM sublattices align antiparallel with each other. Spinel ferrites, iron garnets, hexaferrites, and RE-TM intermetallic compounds are some examples.[4–6]

Recently, new oxyborates $Me_2Me'BO_5$, where *Me* and *Me'* are both TM, have attracted attention as perspective ferrimagnets.[7–10] The TM ions occupying crystallographically nonequivalent sites form individual sublattices and provide different contributions to the total magnetization. A novel nickel oxyborate $Ni_{5.33}Nb_{0.67}B_2O_{10}$ possesses both the magnetization compensation point (T_{comp} = 30 K), which corresponds to the cancellation of the magnetizations of antiparallel-coupled Ni sublattices, and the magnetic phase transition point (T_N = 165 K).[11] The reversal magnetization and exchange bias are also observed in the FM/AFM exchange-coupled sublattices in $Ni_5GeB_2O_{10}$ [12] and Ni_2MnBO_5.[13]

Among the oxyborates, the homometallic Co_3BO_5 material takes a special place. This material is a strongly anisotropic ferrimagnet with Néel temperature T_N = 42 K.[14–17] The Co^{3+} ions occupy one of the fourth octahedral sites (M4) and are in a low-spin state (S = 0), while the high-spin Co^{2+} ions (S = 3/2) fill the M1, M2, and M3 octahedral sites and determine the ferrimagnetic properties (Fig. 1). Due to all magnetic moments being nearly parallel to the *b*-axis the system exhibits strong easy-axis anisotropy as revealed by neutron powder diffraction and bulk magnetization measurements.[18,19]

Being a ferrimagnetic insulator with high axial anisotropy, this material can be considered as a component of spintronic devices. Upon heating, at ~500 and 700 K, the Co_3BO_5 material undergoes electronic transitions associated with the spin-state transformation of cobalt ions at the M4 site.[20] These electronic transitions detected by X-ray diffraction also manifest them-

[a]*Kirensky Institute of Physics, Federal Research Center KSC SB RAS, 660036 Krasnoyarsk, Russia. E-mail: nat@iph.krasn.ru*
[b]*Instituto de Nanociencia y Materiales de Aragón, CSIC-Universidad de Zaragoza and Departamento de Física de la Materia Condensada, 50009 Zaragoza, Spain*
[c]*Servicio de Medidas Físicas, Universidad de Zaragoza, 50009 Zaragoza, Spain*
[d]*Reshetnev Siberian State University of Science and Technology, 660037 Krasnoyarsk, Russia*

†Electronic supplementary information (ESI) available: Intermediate temperature hyperfine parameters; and lattice parameters and unit-cell volumes calculated from the DFT-optimized structures. See DOI: 10.1039/d1dt00125f

‡Deceased.

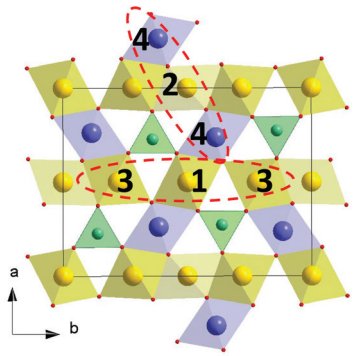

Fig. 1 Crystal structure of $Me_2^{2+}Me'^{3+}BO_5$ presenting the *ab* plane. Four symmetry different metal sites 2a, 2b, 4g, and 4h are numbered as M1, M2, M3, and M4, respectively. The Me^{2+} and Me^{3+} ions are shown as yellow and blue spheres, respectively. The planar triangular BO_3 groups are shown in green. The triads M3–M1–M3 and M4–M2–M4 are depicted by red dotted lines.

selves in the temperature dependences of electrical resistivity[21] and heat capacity,[20] revealing well-defined anomalies. The GGA + U calculations have revealed a metallic ground state at high temperatures.[20]

In Co_2FeBO_5, the replacement of diamagnetic Co^{3+} ions by magnetic Fe^{3+} induces a fascinating transformation in the ferrimagnetic properties. First of all, the enhancement of the antiferromagnetic interactions results in an almost twofold increase in the ferrimagnetic transition temperature (T_{N2} = 70 K) and the appearance of additional antiferromagnetic transition at T_{N1} = 114 K.[22–24] Despite the axial anisotropy inherent to Co_3BO_5 remains, the remanent magnetization is dramatically reduced. Moreover, the Fe-substitution induces an extraordinary magnetic hardness and an increase in the coercive field. The antiferromagnetic coupling between the Co and Fe sublattices could explain the observed compensation of the magnetic moment. Indeed, the recent elemental selective XMCD measurements at Co(K) and Fe(Fe) edges showed that Co and Fe form two sublattices that are aligned antiparallel at low temperatures.[20] Thus, it becomes clear that the Me^{3+} ion plays a crucial role in the charge and magnetic balances, determining the unique electronic and magnetic properties of new ferrimagnets.

The present work is devoted to the experimental and theoretical study of the electronic and magnetic states of Fe ions in Co_2FeBO_5. The compound has an orthorhombic symmetry (sp.gr. *Pbam*(no.55)) with lattice parameters a = 9.3818 Å, b = 12.3445 Å, c = 3.0578 Å, and V = 354.13 Å^3 and crystallizes in the ludwigite structure.[24] The magnetic ions at the M2 and M4 sites and at the M1 and M3 sites form triads with the shortest (4–2–4) and longest (3–1–3) interionic distances, respectively (Fig. 1). These triads propagating along the *c*-axis build spin three-leg ladders.[22,24] Note that previous specific-heat measurements of Co_2FeBO_5 did not reveal any anomalies besides the magnetic ones, and no structural transformations were found up to 150 K.[22] Here, we performed ^{57}Fe Mössbauer effect measurements in the wide temperature range of 4.2–300 K and found that the spectral components (high-spin Fe^{3+} ions) undergo splitting below 117 K due to the magnetic hyperfine fields. A great difference in the quadrupole splittings has been found, which reflects the different ligand contributions to the electrical field gradient (EFG) in the Fe nucleus. We calculated the electronic structure and magnetic moments of the Fe and Co atoms at different metal sites for the three models of Fe cation distributions using density-functional theory (DFT + GGA). Our calculations have revealed that the ground state corresponds to the cation distribution with high-spin Fe^{3+} ions exclusively filling the M4 site and high-spin Co^{2+} ions located at the M1, M2, and M3 sites. Other Fe distributions cause an increase in the ligand contributions to EFG. Moreover, our calculations show that a ground state is ferrimagnetic with the Co and Fe magnetic moments being nearly parallel to the *b*-axis and antiparallel to each other. The total magnetic moment was found to be *circa* 1.1μ_B f.u.$^{-1}$, which is in good agreement with the experimental value. The magnetic anisotropy is defined by the intrinsic electronic structure of the systems.

2. Experimental and theoretical techniques

The investigated crystals of Co_2FeBO_5 were grown by L. N. Bezmaternykh using the flux method. The details of synthesis are given in ref. 24. For the Mössbauer effect experiment we used a powder of crushed single crystals. The Mössbauer absorption spectra of ^{57}Fe nuclei were recorded in the temperature range between 4.2 and 300 K with a standard MS-1104Em spectrometer operating in the constant acceleration regime and a Gifford-McMahon cryostat on a closed-cycle helium refrigerator. The gamma-ray source ^{57}Co(Cr) was used at room temperature. The sample was fixed in a polymer iron-free holder so that it was perpendicular to the propagation direction of gamma rays. The isomer shifts of the Mössbauer spectra were measured relative to a metal α-Fe standard absorber. The hyperfine parameters were obtained by the least-squares procedure assuming the Lorentzian line shapes. The details of the calculations of the probabilities of the quadrupole splittings ($P(QS)$) and hyperfine fields ($P(H_{hf})$) are described in the ESI.† A small amount of spurious phase, which is at the detection limit (A = ±3%), was found. This component which is better defined in the 4.2 K spectrum (Fig. 1S, ESI†) as a paramagnetic doublet with parameters IS = 0.21 mm s^{-1}, QS = 0.55 mm s^{-1}, and W = 0.38 mm s^{-1} is probably due to an impurity, which accidentally got into, as a result of grinding. Its contribution was subtracted from the spectra to finally yield the Co_2FeBO_5 ludwigite spectrum.

The electronic structure of Co_2FeBO_5 was calculated using density-functional theory (DFT) in the generalized gradient approximation (GGA), where the exchange–correlation functional is chosen within the Perdew–Burke–Ernzerhof (PBE) parametrization.[27] The calculations were performed using the

Vienna *Ab initio* Simulation Package (VASP)[28] with projector augmented wave (PAW) pseudopotentials.[27] The valence electron configurations of $3d^6 4s^2$, $3d^7 4s^2$, $2s^2 2p^4$, and $2s^2 2p^1$ were taken for the Fe, Co, O, and B atoms, respectively. The plane-wave cutoff energy was 600 eV. The Brillouin-zone integration was performed on a 3 × 2 × 8 Monkhorst–Pack grid[29] of special points. The electric field gradient was calculated within the scheme suggested in ref. 30. The SCAN functional was used for treating the transition metal atoms.[31] The crystal structure obtained at room temperature[24] was used as the initial guess and then the lattice parameters and atomic coordinates were optimized. The optimized lattice parameters and atomic coordinates were obtained by minimizing the total energy.

3. Results and discussion

3.1. The Mössbauer effect

The room-temperature Mössbauer spectrum of the Co_2FeBO_5 ludwigite presents the sum of several symmetric quadruple doublets (Fig. 2a). The calculated probability of the quadrupole splitting $P(QS)$ shows four maxima in the range of 0.5–2.0 mm s^{-1} which can be attributed to the nonequivalent iron sites with different local crystal and cation neighboring environments (Fig. 2b). The maxima positions were used for the model spectra calculations. Then the whole set of hyperfine parameters was varied to combine the model and experimental spectra in the frame of the least-squares method in the linear approximation. As a result, the Mössbauer spectrum at room temperature can be satisfactorily fitted to a four-doublet model with the hyperfine parameters listed in Table 1. It is clearly seen that all doublets with the isomer chemical shifts $IS \approx 0.39 \pm 0.01$ mm s^{-1} can be assigned to high-spin Fe^{3+} ions with octahedral oxygen coordination. Also, there is a great difference in the quadrupole splitting values, which are $QS1$ = 1.92 ± 0.02, $QS2$ = 1.11 ± 0.02, $QS3$ = 0.90 ± 0.02, and $QS4$ = 0.62 ± 0.02 mm s^{-1}. The area ratio of the four components was found to be $A1 : A2 : A3 : A4 = 0.10 : 0.55 : 0.24 : 0.11$. The isomer shift IS and quadrupole splitting QS evaluated for all four spectral components in the paramagnetic phase are plotted in Fig. 3 as a function of temperature. The isomer shifts show a gradual increase in accordance with the second-order Doppler shift. The quadrupole splitting is nearly independent of temperature for all the components, which is in agreement with the expectation for Fe^{3+} (HS) with its symmetrical d^5 configuration.

We started the analysis of magnetic Mössbauer spectra from 4.2 K, where the absorption lines are sharp and well resolved (Fig. 4a). The spectral profile still suggests four components for an adequate fitting of the data (Table 1). An analysis in terms of the distribution function of magnetic hyperfine fields reveals evidence of splitting into distinct components. The $P(H_{hf})$ curve obtained at 4.2 K shows four resolved maxima in the interval of 480–550 kOe and small con-

Table 1 The hyperfine structure parameters for Co_2FeBO_5. IS – isomer chemical shift with respect to αFe (±0.01 mm s^{-1}), H_{hf}. –hyperfine field (±10 kOe), QS and 2ε – quadruple splitting (±0.02 mm s^{-1}) defined by eqn (1) and (2) in the paramagnetic and magnetic regimes, respectively. W is the half-line width (±0.06 mm s^{-1}), A is the area of the corresponding component (the iron occupation factor) (±0.03 a.u.)

T (K)		IS (mm s^{-1})	QS, 2ε (mm s^{-1})	H_{hf} (kOe)	W (mm s^{-1})	A (a.u.)
300	D1	0.40	1.92		0.36	0.10
	D2	0.37	1.11		0.36	0.55
	D3	0.38	0.90		0.27	0.24
	D4	0.40	0.62		0.27	0.11
4.2	S1	0.53	1.79	517	0.35	0.26
	S2	0.52	0.28	528	0.41	0.31
	S3	0.50	0.43	512	0.43	0.32
	S4	0.47	−1.85	474	0.88	0.12

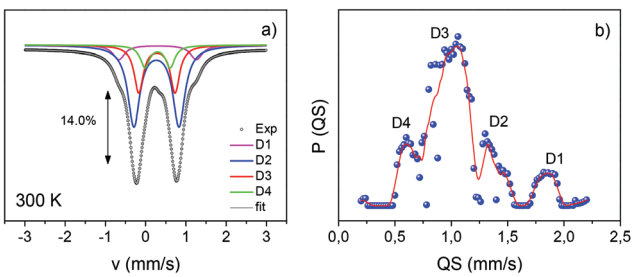

Fig. 2 (a) The room-temperature Mössbauer spectra of Co_2FeBO_5. Solid lines indicate the calculated spectral components. The absorption scale is shown in %. (b) The appropriate probabilities of quadruple splitting $P(QS)$ calculated from the experimental spectrum. The solid red line is the curve obtained by averaging over three points.

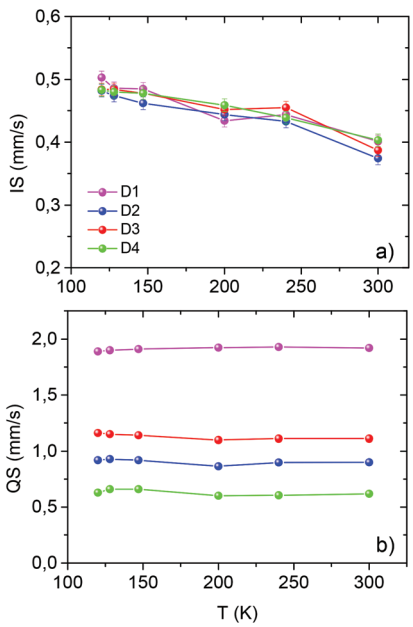

Fig. 3 The temperature variation of (a) the isomer shift (IS) and (b) the quadrupole splitting (QS). Unless shown, error bars are commensurate with the symbol size.

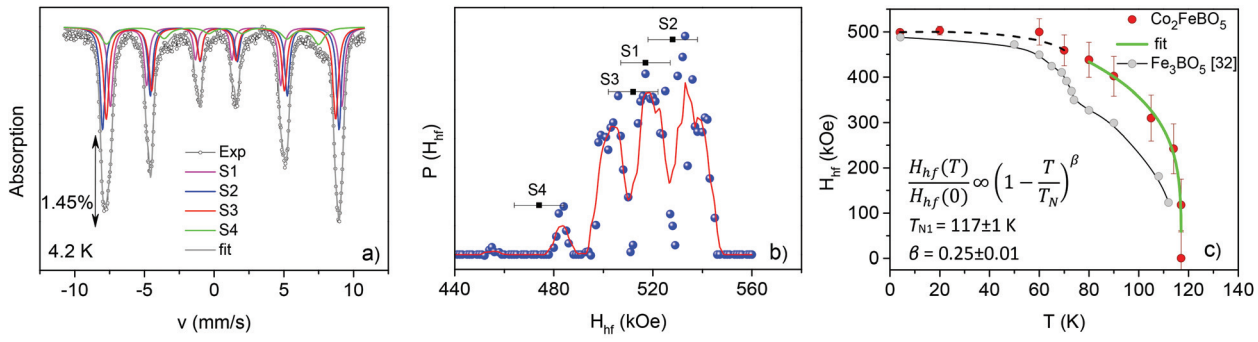

Fig. 4 (a) Mössbauer spectrum of Co_2FeBO_5 at T = 4.2 K. The solid lines S1, S2, S3, and S4 indicate the calculated spectral components corresponding to the high-spin Fe^{3+} ions. The absorption scale is shown in %. (b) The distribution of hyperfine fields showing four distinct maxima in the interval of 450–550 kOe. The values of the hyperfine fields are shown by square symbols with error bar. The solid red line is the curve obtained by averaging over three points. (c) Temperature dependence of the average hyperfine field $\langle H_{hf} \rangle$. The green solid line near T_N is the fit using the scaling model. The dashed line is a guide for the eye. Data for Fe_3BO_5 taken from ref. 32 are shown.

tributions from the other distributions (Fig. 4b). The isomer shift values *IS*1, *IS*2, *IS*3, and *IS*4, although increased ~0.5 mm s^{-1}, are in the typical range of the high-spin Fe^{3+} ion. So, the spectrum at the lowest measured temperature can be reasonably approximated by four sextets with close values of the isomer shifts *IS*, but different values of the hyperfine fields H_{hf}: 517 (S1), 528 (S2), 512 (S3), and 474 (S4) ± 10 kOe. These values seem rather typical of the Fe^{3+} ion in the high-spin state and are in good agreement with those of 488 kOe (Douvalis *et al.*[32]) and ~500 kOe (Larrea *et al.*[33]) observed in Fe_3BO_5 for the localized Fe^{3+} state at the M4 site and also with those of 468 kOe (Continentino *et al.*[7]), 510 kOe (Fernandes *et al.*[34]), and an average field of 451 kOe (Wiedenmann *et al.*[35]) observed in Cu_2FeBO_5, Ni_2FeBO_5, and Mg_2FeBO_5, respectively. The average hyperfine field $\langle H_{hf}(4.2\ K) \rangle \approx 508$ kOe observed in Co_2FeBO_5 is about ~90% of the value observed in $FeBO_3$ at the same temperature,[36] indicating that the system is almost magnetically saturated. This result is consistent with a hysteresis loop recorded by XMCD at the Fe(K-edge) with a clear sign of saturation.[20]

All components undergo magnetic splitting in the range of 114–120 K (Fig. 5). In the vicinity of the magnetic transition temperature, the line-widths of the Mössbauer spectra (W) become broadened. The broadening of the outer lines (1–6) is much higher than that of the inner lines (3 and 4). It is quite remarkable that the spectra even at 80 K, *i.e.* well below T_{N1}, are still so broad. In the intermediate temperature range, the actual distribution pattern of H_{hf} is complex and the four components are not defined unambiguously. It can be caused by the irregular Fe cation environment in the ludwigite lattice. In addition, a random distribution of superexchange interactions on Fe ions due to the magnetic frustrations is possible,[17] which Mössbauer spectroscopy highly senses as line broadening. We actually observed a significant decrease in the speed of the spectra recording in the intermediate temperature range, which is most likely due to the line broadening when the intensity of the broad H_{hf} distribution is spread over a larger velocity range and the required data collection times increase.

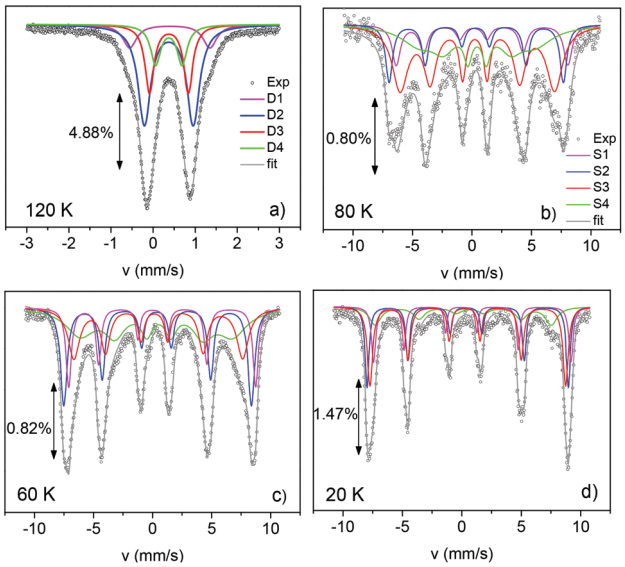

Fig. 5 Mössbauer spectra of the Co_2FeBO_5 ludwigite obtained at 120 K (a), 80 K (b), 60 K (c), and 20 K (d). The color lines show different spectral components. The absorption scale is shown in %.

The temperature variation of the average hyperfine field $\langle H_{hf} \rangle$ is shown in Fig. 4c. The same dependence of H_{hf} for the Fe^{3+} ions occupying the M4 site in Fe_3BO_5 is also displayed.[32] Both compounds demonstrate close magnitudes of hyperfine fields at T = 4.2 K and a rapid decrease in H_{hf} in the range T = 115–120 K, indicating that magnetic ordering of iron nuclei occurs. For Co_2FeBO_5 the temperature transition extracted using the scaling model (T_{N1} = 117 ± 1 K) agrees well with that found from the macroscopic magnetization study.[22,24] However, there is a distinctive feature of the behavior of the two materials – the hyperfine field in Co_2FeBO_5 does not show any inflection or jump at T_{N2} = 70 K in contrast to Fe_3BO_5. Previously, a similar behavior of $H_{hf}(T)$ was observed in Ni_2FeBO_5 and was associated with the independent ordering of the magnetic subsystems Ni^{2+} and Fe^{3+}.[34]

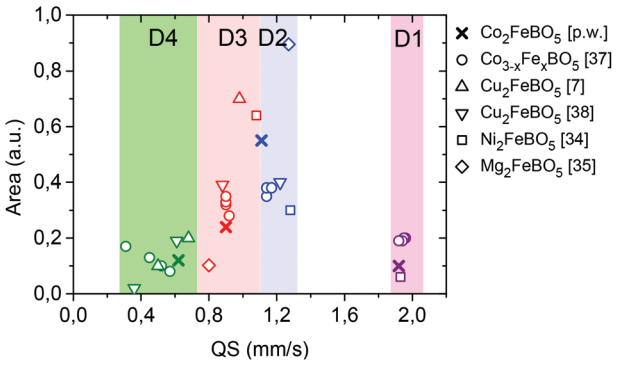

Fig. 6 The area of spectral components for different quadrupole splittings (*QS*) obtained for Fe-containing ludwigites. All data correspond to the paramagnetic regime (T = 300 K). The intervals of quadrupole splitting for doublets D1, D2, D3, and D4 are highlighted in different colors.

From Fig. 6, it is seen that the Fe^{3+} ions in Co_2FeBO_5 show the *QS* values in line with the reported data for Fe-containing ludwigites.[32–35,37,38] The quadrupole splitting values fall in the ranges 1.97–1.90 mm s^{-1} (D1), 1.30–1.10 mm s^{-1} (D2), 1.10–0.70 mm s^{-1} (D3), and 0.70–0.30 mm s^{-1} (D4). The spectral components D2 and D3 show the largest areas, while the areas of D1 and D4 components do not exceed 0.20 for all compounds studied. The examination of the $Co_{3-x}Fe_xBO_5$ system ($0.0 < x \leq 1.0$) shows that the areas of D1 and D4 doublets rapidly decrease with a further increase in the Fe concentration, whereas an opposite trend is seen for D2 and D3 components, the areas of which increase with the Fe content. So, one can conclude that in the ludwigites the iron ions are not distributed randomly over the lattice sites, but occupy certain sites, the filling of which depends on the concentration.

The value of quadruple splitting *QS*1 is very high, which indicates a very large distortion of the oxygen octahedron occupied by Fe^{3+} ion. This value is comparable with the value of *QS* = 1.89–2.06 mm s^{-1} reported for the iron-rich epidotes $A_2M_3Si_3O_{12}OH$, where A^{2+} = Ca and Sr and M^{3+} = Al, Fe, and Mn.[39] In epidotes, the high-spin Fe^{3+} ions occupy the strongly distorted octahedral site and the valence contribution due to the Fe(3d) shell anisotropy was found to be the largest contribution to *QS*, as it follows from the cluster molecular orbital calculations in local spin-density approximation.[39]

The values of quadrupole splittings *QS*2 and *QS*3 are close and lie between those observed for the localized Fe^{3+} ion at the M4 site (~0.78 mm s^{-1} and ~1.27 mm s^{-1} found in Fe_3BO_5,[32] Cu_2FeBO_5,[7] Ni_2FeBO_5,[34] and Mg_2FeBO_5).[35] The comparison of the values of the hyperfine fields for S2 and S3 sextets with those of other ludwigites shows that they are also typical of Fe^{3+} ions located at the M4 site.

Note that in the paramagnetic phase, the observed quadrupole splitting is given by the relation

$$\mathrm{QS} = \frac{1}{2}|eQV_{zz}|\left(1+\frac{\eta^2}{3}\right)^{1/2} \quad (1)$$

where Q is the nuclear quadrupole moment of the excited state of ^{57}Fe, V_{zz} is the main component of the electric field gradient (EFG) tensor, and $\eta = (V_{xx} - V_{yy})/V_{zz}$ ($|V_{zz}| \geq |V_{yy}| \geq |V_{xx}|$) is an asymmetry parameter describing the deviation from axial symmetry. The numerical factor due to this parameter equals 1 for the axially symmetric EFG (η = 0.0) and 1.15 for maximally asymmetric EFG (η = 1.0). In the paramagnetic phase the sign of V_{zz} and thus of *QS* cannot be determined as the intensities of the two doublet components are the same in the case of a random powder. On the other hand, in the magnetically ordered phase, the quadrupole splitting depends on the direction of the hyperfine field relative to the main component of the tensor of electrical field gradient:

$$2\varepsilon = \frac{1}{2}eQV_{zz}\frac{(3\cos^2\Theta - 1)}{2} \quad (2)$$

where Θ is the angle between the directions of H_{hf} and V_{zz}.

In the magnetically ordered phase, the quadrupole splittings of Co_2FeBO_5 reveal a high sensitivity to the temperature effect (Table 1). At 4.2 K the visible quadrupole splitting shows a decrement for the S2 and S3 components and becomes negative for the S4 one. It is rather unlikely that there is a major change in the local symmetry of octahedral coordination and hence, the *QS* parameter of any of the components. Such a change in the quadrupole splitting is most likely due to the angle factor ($3\cos^2\Theta - 1$). The interpretation of the quadrupole splitting parameter in the magnetically ordered phase requires knowledge of the crystal structure and the Θ parameter. This issue will be addressed by the theoretical calculations below.

3.2. DFT–GGA calculations

To gain further insights into the electronic and magnetic states of Fe ions in a Co_2FeBO_5 single crystal we have performed *ab initio* calculations of the electronic and magnetic structures for different cation distributions. The Mössbauer effect studies and resonant powder X-ray diffraction experiment[39] demonstrate an evident preference of Fe^{3+} ions to occupy the M4 site. It is quite reasonable, therefore, to assume that in Fe-substituted ludwigites the M4 site would be filled firstly and cation distribution order of M4 > M2 ≫ M3 ≈ M1 would be fulfilled. We calculated the properties of Co_2FeBO_5 for three distributions of Fe^{3+} ions over the crystallographically nonequivalent metal sites M2 and M4. The first distribution corresponds to the Fe^{3+} ions occupying the M4 site exclusively. We marked it as "Fe4(HS)", where HS denotes the high-spin state. The second one assumes that Fe^{3+} ions are distributed over the 4–2–4 triad, thereby filling both the M2 and M4 sites. This is a "Fe4–Fe2–Fe4" case. And the third model is a modified first model, where some amount of Fe^{3+} ions located at the M4 site are in the low-spin state (LS), "Fe4(HS,LS)". For a qualitative description of this model, we used a 2 × 2 × 1 ordered supercell containing 12.5% Fe atoms in the low-spin state.

From the DFT–GGA calculations, we have estimated the lattice parameters and unit-cell volumes at T = 0 K for all three

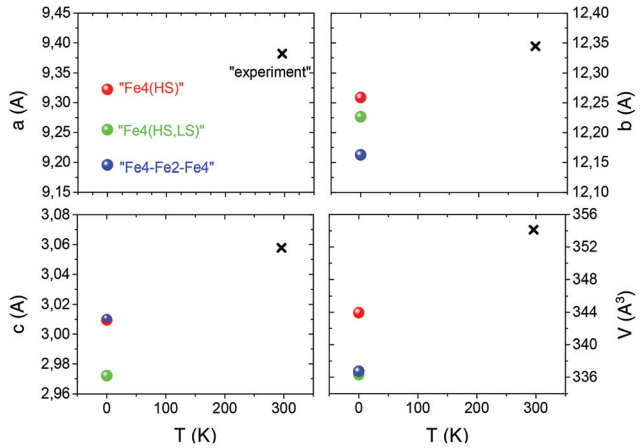

Fig. 7 Lattice parameters and unit-cell volume for Co_2FeBO_5. The values calculated from the DFT-optimized structure for the "Fe4(HS)", "Fe4(HS,LS)", and "Fe4–Fe2–Fe4" models at T = 0 K are marked by red, green, and blue circles, respectively, and the values obtained from the single crystal X-ray diffraction experiment at T = 296 K (ref. 24) are shown by black crosses. The symbol size is larger than the error bar.

cases (Fig. 7 and Table S2, ESI†). For all the calculated structures we have obtained the orthorhombic symmetry with the space group *Pbam*. It turns out that for the "Fe4(HS)" model the DFT-optimized unit-cell parameters are in much better agreement with the experimental parameters[24] than for the other two distribution models. So, for the "Fe4(HS)" distribution the relative difference between the calculated and experimental volumes is only ~3%, while for the "Fe4(HS,LS)" and "Fe4–Fe2–Fe4" cases it is about 5%. The next observation is that the *c*-parameter is very sensitive to the spin state of the cation at the M4 site. The HS to LS transformation of a part of the Fe^{3+} ions located at the M4 site leads to a sharp decrease in the *c*-parameter, while *a*- and *b*-parameters show a more monotonic reduction. It can be explained by the fact that the Fe^{3+} ions in the LS state have a smaller ionic radius r_i^{LS} = 0.690 Å instead of r_i^{HS} = 0.785 Å according to Shannon.[40] Previously we have observed a similar behaviour of lattice parameters for the Co-based ludwigites.[20]

We calculated the total energies of all three structures and found that the ferrimagnetic configuration M1(↓)M2(↑)M3(↑)M4(↓) has the lowest energy for each of the three models, where ↑ stands for spin up and ↓ for spin down and the order of numbers corresponds to the metal sites in the Co_2FeBO_5 ludwigite. The next important result is that if Fe^{3+} ions fill the M4 site exclusively ("Fe4(HS)") then this cation distribution has the lowest total energy among all the considered cases. The "Fe4–Fe2–Fe4" and "Fe4(HS,LS)" cases are higher in energy by 354 and 398 meV per cell or ~89 and 95 meV per Fe ion, respectively. These energy differences are about ~9% of the ground state energy "Fe4(HS)" and, hence, one may expect that these cation distributions can be realized as a spurious cation disorder.

It is reasonable to begin the analysis of the electronic and magnetic structures of Co_2FeBO_5 with the model of "Fe4(HS)" since it can be considered as the ground state. The plots of the partial density of states (pDOS) for this model are shown in Fig. 8. The largest hybridization is between the O 2p and B 2p states and is observed over the whole energy range. The states inside the triangular BO_3 groups undergo the strongest covalent interaction. The B 2p states provide a predominant contribution to the bands of 3 eV above the Fermi level and mainly form the conduction band. The exchange splitting between the spin-up and spin-down Co 3d and Fe 3d states were estimated to be 0.4 eV for Co1, 0.5 eV for Co2, 0.4 eV for Co3, and 0.5 eV for Fe4. All metal ions were found to be in the strongly distorted octahedra with the crystal field splittings of 0.05–0.10 eV, which are lower than the exchange splitting and, hence, well consistent with the high-spin state of Co and Fe ions. It is noteworthy that there is a pairwise hybridization of the d orbitals of Co and Fe belonging to different metal sites. The Co1, Co3 and Co2, Fe4 (the t_{2g} and e_g) states with opposite spin projections share nearly the same energy intervals. The higher part of the valence band is mainly formed by Co 3d and Fe 3d states hybridized with O 2p states. The relative strength of Fe 3d–O 2p hybridization of σ and π type is smaller than that for the Co 3d states. The Fe 3d density of states reveals narrower peaks than for Co 3d, indicating somewhat a smaller covalent mixing of these orbitals with the occupied oxygen ones. Fig. 8e shows the energy interval near the Fermi level in zoom. It can be seen that the partially occupied bands crossing the Fermi level are formed by majority spin Fe4 (t_{2g} and e_g) and Co1 (t_{2g}) states. Thus, a metallic ferrimagnetic solution with partially filled bands at the Fermi level was obtained within our GGA–PBE approach, while the resistivity measurements directly indicated the insulating properties.[25,26] This discrepancy results from inadequate treatment of strong electron correlations typical of 3d-metal oxides which form the Mott-Hubbard insulator state. The Fermi level in Fig. 8e is only 0.1 eV below the top of the valence band. The simplest GGA+correction shifts the Fermi level in the insulator gap.

The spin moments per Co and Fe ion calculated for the three cation models are listed in Table 2. The absolute values of magnetic moments are consistent with those expected for high-spin and low-spin states. For the ground-state magnetic configuration "Fe4(HS)" (↓↑↑↓) we additionally carried out the GGA + SOC calculations taking into account the spin–orbit coupling. SOC does not change considerably the charge and spin states of Co and Fe ions but results in the magnetic moments to be directed mostly along the *b*-axis for all metal sites. The spin moments are

$$m_s^{Co1} = (\pm 0.04, -2.36, \pm 0.1)\mu_B,$$

$$m_s^{Co2} = (\pm 0.01, +2.40, \pm 0.2)\mu_B,$$

$$m_s^{Co3} = (\pm 0.05, +2.48, \pm 0.02)\mu_B,$$

$$m_s^{Fe4} = (\pm 0.1, -3.60, \pm 0.2)\mu_B,$$

where the signs correspond to different ions in the same crystallographic class (there are two Co1, two Co2, four Co3, and

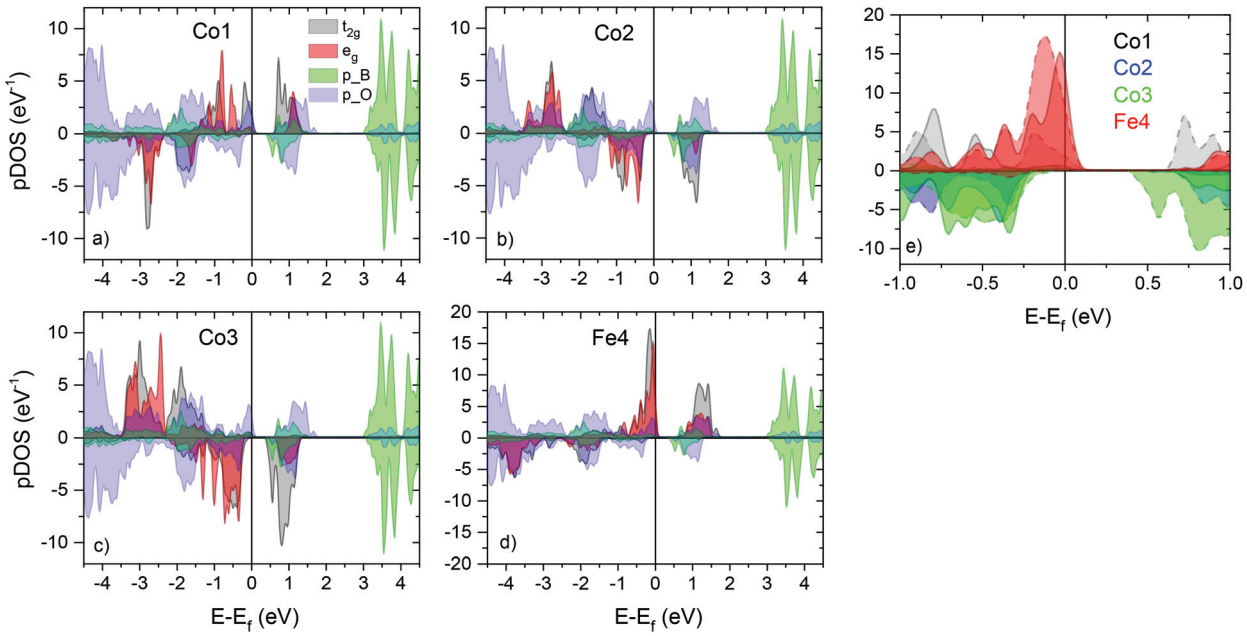

Fig. 8 Partial density of states (pDOS) for Co1 (a), Co2 (b), Co3 (c), and Fe4 (d) and for the B and O atoms calculated for the "Fe4(HS)" model of the cation distribution. The Fermi level is shown by a black solid line. The positive and negative values of pDOS for Co and Fe correspond to the spin-up and spin-down, respectively. The density of states for B is increased by a factor of 10 for clarity. (e) The partial DOS for Co and Fe cations near the Fermi level. The t_{2g} and e_g states are shown by the dotted and solid lines, respectively.

Table 2 The d-shell occupation n_d, spin magnetic moments m (μ_B), an asymmetry parameter η, and a ligand contribution to EFG V_{zz} (V m^{-2}) for the distinct metal sites in Co_2FeBO_5 obtained for different Fe distributions in DFT + GGA calculations

	"Fe4(HS)"					"Fe4–Fe2–Fe4"					"Fe4(HS,LS)"				
Atom	n_d	m (μ_B)	η	$V_{zz}\times10^{21}$ (V m^{-2})	Θ (grad)	Atom	n_d	m (μ_B)	η	$V_{zz}\times10^{21}$ (V m^{-2})	Atom	n_d	m (μ_B)	η	$V_{zz}\times10^{21}$ (V m^{-2})
Co1	7.2	−2.44	0.79	3.76	12.5	Co1	7.2	−2.45	0.22	4.87	Co1	7.2	−2.37	0.84	4.00
Co2	7.1	2.46	0.91	1.88	88.8	Co2	7.1	2.52	0.63	6.00	Co2	7.1	2.44	0.92	2.12
						Fe2 (LS)	6.5	0.49	0.88	4.17					
Co3	7.1	2.50	0.67	4.30	41.5	Co3	7.1	2.40	0.53	4.80	Co3	7.1	2.48	0.67	4.96
						Co4	7.0	−2.24	0.02	−5.80					
Fe4(HS)	5.9	−3.58	0.004	−1.20	88.8	Fe4(HS)	5.9	−3.57	0.06	−4.30	Fe4(HS)	5.9	−3.56	0.08	−3.04
											Fe4(LS)	6.1	−0.70	0.21	1.44

four Fe4 atoms in the unit cell). We also found that the orbital moments are parallel to the spin moments and are m_l ~0.15–0.30μ_B for Co ions and ~0.06μ_B for Fe ions. The unquenched orbital moment is rather typical of various oxides based on the Co^{2+} ions. Our calculations provide an explanation of the following experimental observations: (i) in Co_2FeBO_5 the Co and Fe magnetic moments are nearly directed along the *b*-axis and, hence make this the easy magnetization axis in accordance with the bulk magnetization measurements.[24] (ii) The ferrimagnetic arrangement of the Co^{2+} magnetic moments is in good agreement with the shape of the magnetization curve of the cobalt sublattice recorded by XMCD at the Co (K-edge), which shows the superposition of ferro- and antiferromagnetic contributions.[20] (iii) Finally, according to our calculations, the total magnetic moment of the Co sublattice along the *b*-axis is ~+2.5μ_B while the magnetic moment of the Fe sublattice is −3.6μ_B and it is oppositely directed. This is in excellent agreement with the result of antiferromagnetic coupling between the Co and Fe sublattices found using XMCD measurements,[20] and with the experimental magnetic moment 0.94μ_B per formula unit found using *dc* magnetization measurements.[24]

To understand the origin of the quadrupole splittings observed in Co_2FeBO_5 (Table 1 and Fig. 6) it is necessary to consider different contributions to *QS*. It is well known that the quadrupole splitting arises from the interaction between the nuclear quadrupole moment and the non-spherical component of the electronic charge distribution described by its effective electrical field gradient. In a simplified model, the EFG can be considered as the sum of two main contributions: the electronic contribution q_{el} from the charge distribution of the non-spherical 3d electronic shell and the lattice contri-

bution q_{lat} arising from the charge distribution of the surrounding ligands. In ferric high-spin compounds the main contribution to the quadrupole splitting arises predominantly from the ligand contribution to EFG, while in ferrous compounds the electronic part of the *QS* predominates.

We calculated the ligand contribution to EFG through the V_{zz} and η parameters for all distribution models (Table 2). Firstly, we found that the substantial tetragonal elongation of the $M4O_6$ octahedron along one of the axes remains independently of the Co or Fe ions occupying this site and the spin state of the latter. Secondly, the local environments of the Co1 and Co3 sites are only slightly changed due to the cation distribution. Thirdly, we found that the ligand contribution to EFG depends on the metal site occupied by Fe^{3+} ions. If the high-spin Fe^{3+} ions occupy the M4 site, "F4(HS) model", then the EFG tensors for all four symmetrically non-equivalent sites are small. In particular, the EFG for the M4 site is the smallest (V_{zz} = −1.20 10^{21} V m^{-2}), negative, and almost axially symmetric with η = 0.004. In contrast, if Fe^{3+} ions are distributed over the 4–2–4 triad, "Fe4–Fe2–Fe4 model", this causes a dramatic increase in the local distortions of these sites. So, the EFG rises to values of V_{zz} (Co2/Fe2) = 6.00/4.17 and V_{zz} (Co4/Fe4) = −5.8/−4.3 10^{21} V m^{-2}. The asymmetry of the local environment of Fe ions increases, as is reflected in the enlarged parameter η. Interestingly, such cation distribution leads to coordinated octahedra in the triads Co3–Co1–Co3, Co4–Co2–Co4, and Fe4–Fe2–Fe4 to become equivalent in size and local distortions, which reflects the indication of a finite cationic and charge order inherent to the "Fe4–Fe2–Fe4" model. In the same model, we obtained an unexpected result, which is the Fe^{3+} ions at the M2 site adopted the low-spin state with a magnetic moment of ∼0.5μ_B (Fe2(LS)), while the Fe^{3+} ions at the M4 site are still in the high-spin state with a moment of 3.57μ_B (Fe4(HS)). Finally, for the third model "Fe4(HS,LS)", the calculation and optimization of the structural parameters were performed under the condition that some amount of iron should remain in the low-spin state. This condition is fulfilled for the Fe4(LS) site with a small magnetic moment of 0.7μ_B. The calculation of EFG tensors revealed that both octahedra become considerably more regular, V_{zz} (Fe4(LS)) = −1.44 10^{21} V m^{-2} and V_{zz} (Fe4(HS)) = −3.04 10^{21} V m^{-2} compared with the "Fe4–Fe2–Fe4" model. This qualitative trend reflects that the low-spin Fe^{3+} ions located at the M4 site, Fe4(LS), induce less ligand contribution to EFG than those at the M2 site, Fe2(LS).

Assuming that no structural changes occur below room temperature, and keeping the value of the constant of quadrupole splitting eQV_{zz} independent of temperature, we have calculated this value for the Fe4(HS) model as a ground state. The size of the nuclear quadrupole moment *Q* of the first excited state of ^{57}Fe is assumed to be 0.16 b. We found the value of eQV_{zz} = −0.40 mm s^{-1}. The electric field gradient is oriented at an angle of 88.8° relative to the magnetic hyperfine field H_{hf}. The obtained quadrupole splitting *QS* = 0.20 mm s^{-1} and 2ε = 0.10 mm s^{-1} lie in the range of the measured values in the paramagnetic and magnetically ordered phases, respectively, for D2 (S2) and D3(S3) components possessing the largest spectral areas. However, these parameters are lower than the experimental values. The reason can be that the calculations rely on the ideal model, whereas in real materials the local environment due to antisite disorder is more distorted which increases *QS* and which also may lead to a variation in the Θ values.

The electronic contribution to EFG can be qualitatively estimated through the anisotropy of the 3d shell, which is expressed as follows: $\Delta n_d = n_{x^2-y^2} + n_{xy} - n_{z^2} - (n_{xz} - n_{yz})/2$. The ferric Fe 3d shell anisotropy is expected to be zero if each of the five 3d orbitals is singly occupied. We found that for all models under consideration, the high-spin Fe^{3+} ions (Fe4(HS)) exhibit a small anisotropy Δn_d due to spin-down electrons, indicating near-spherical symmetry of the charge distribution (Table S3, ESI†). In contrast, spin-up electrons yield a large anisotropy Δn_d and, hence they should contribute to EFG. The valence contribution to EFG arises from the admixtures of the formally empty spin-up 3d orbitals to the occupied O 2p states. It is obvious that the t_{2g} contribution is the same for all models, while the main difference is due to the differences in the occupation of the e_g orbitals.

Although the results obtained do not allow the direct assignment of the Mössbauer components D1, D2, D3, and D4 to particular crystallographic sites, they clearly show that the most probable iron ion distribution is when Fe^{3+} ions are in the high-spin state and fill site 4, creating the smallest ligand contribution to EFG. The appearance of Fe^{3+} ions in the other crystallographic sites or in the other spin-state (LS in a given case) leads to a sharp change in local distortions and, as a consequence, in the ligand contributions. Referring to the calculations one may mainly expect some M2–M4 antisite disorder which in course would lead to a local variation in the coordination environments of the Fe^{3+} ions which could explain the quite complex $P(QS)$ and $P(H_{hf})$.

4. Conclusions

The electron and magnetic states of Fe ions in the Co_2FeBO_5 ludwigite have been studied using Mössbauer spectroscopy. The room-temperature spectrum is composed of four paramagnetic components corresponding to the high-spin Fe^{3+} ions in octahedral oxygen coordination. As temperature decreases all components undergo magnetic splitting with a transition temperature T_{N1} = 117 K.

The values of the quadrupole splittings observed at room temperature (*QS*1 = 1.92 mm s^{-1}, *QS*2 = 1.11 mm s^{-1}, *QS*3 = 0.90 mm s^{-1}, and *QS*4 = 0.62 mm s^{-1}) lie in the ranges of the values reported earlier for Fe-containing ludwigites and fit into the concentration dependence found for solid solutions $Co_{3-x}Fe_xBO_5$ ($0.0 < x \leq 1.0$).[32–35,37,38] Combining the present data with those of previous studies it is obvious that in the Co_2FeBO_5 ludwigite there is a well-differentiated set of quadrupole splittings corresponding to the non-equivalent iron sites. This clearly indicates that iron ions are not distributed randomly over the lattice sites, but occupy certain crystallographic positions, the filling of which depends on the concentration.

Our DFT + GGA calculations reveal that the cationic distribution model "Fe4(HS)" is a ground state. Its structural parameters and local geometry are in best agreement with the experimental results.[22,24] According to this model, all Fe^{3+} ions are in the HS state and occupy position M4. In comparison with the Mössbauer spectroscopy result, this result suggests that the doublets with the largest area (D2 and D3) correspond to this distribution. The calculated quadrupole splitting shows that this model yields satisfactory results with QS = 0.20 mm s^{-1} for the paramagnetic phase and 2ε = 0.10 mm s^{-1} for the magnetically ordered phase, which are in good agreement with the measured values. The energies of the other two models "Fe4–Fe2–Fe4" and "Fe4(HS,LS)" are slightly higher and, therefore they can be considered as random distributions resulting from cationic disorder. Such disorder can arise during synthesis, at high temperatures. In these models, iron atoms, in addition to the M4 position, can occupy the M2 position and adopt the low-spin state. If such distributions are realized, then their presence can be detected through the increased/decreased values of the ligand contribution to the electric field gradient compared to those values found for the ground state. Examples of such distributions can be doublets of D1 and D4.

Finally, the calculation predicts that Co_2FeBO_5 is a ferrimagnet with antiferromagnetically coupled Co and Fe magnetic moments and directed nearly parallel to the *b*-axis making it the easy-magnetization direction. These conclusions are consistent with the results of the bulk magnetization and XMCD measurements.

Conflicts of interest

There are no conflicts to declare.

Acknowledgements

The authors acknowledge Prof. I. S. Lyubutin for helpful discussions and a critical reading of the manuscript. This research is funded by the Russian Foundation for Basic Research (project no. 20-02-00559 and 21-52-12033), the Russian Foundation for Basic Research, Government of Krasnoyarsk Territory, Krasnoyarsk Regional Fund of Science (project no. 19-42-240016) and the President Council on Grants (project no. MK-2339.2020.2). The authors acknowledge financial support from the Spanish Ministry of Economy, Industry and Competitiveness (MINECO Grant No. MAT2017-83468-R and from the regional Government of Aragón (E12-20R RASMIA project).

Notes and references

1 S. K. Kim, Fast and efficient switching with ferrimagnets, *Nat. Electron.*, 2020, **3**, 18–19, DOI: 10.1038/s41928-019-0352-9.

2 S. A. Siddiqui, J. Han, J. T. Finley, C. A. Ross and L. Liu, Current-induced domain wall motion in a compensated ferrimagnet, *Phys. Rev. Lett.*, 2018, **121**(5), 057701, DOI: 10.1103/PhysRevLett.121.057701.

3 T. Ostler, J. Barker, R. Evans, *et al.*, Ultrafast heating as a sufficient stimulus for magnetization reversal in a ferrimagnet, *Nat. Commun.*, 2012, **3**, 666, DOI: 10.1038/ncomms1666.

4 C. D. Stanciu, F. Hansteen, A. V. Kimel, A. Tsukamoto, A. Itoh, A. Kirilyuk and T. Rasing, Ultrafast interaction of the angular momentum of photons with spins in the metallic amorphous alloy GdFeCo, *Phys. Rev. Lett.*, 2007, **98**(20), 207401, DOI: 10.1103/PhysRevLett.98.207401.

5 S. Emori and P. Li, Ferrimagnetic insulators for spintronics: Beyond garnets, *J. Appl. Phys.*, 2021, **129**(2), 020901, DOI: 10.1063/5.0033259.

6 S. V. Trukhanov, A. V. Trukhanov, V. G. Kostishyn, L. V. Panina, A. V. Trukhanov, V. A. Turchenko, D. I. Tishkevich, E. L. Trukhanova, O. S. Yakovenko and L. Y. Matzui, Investigation into the structural features and microwave absorption of doped barium hexaferrites, *Dalton Trans.*, 2017, **46**(28), 9010–9021, DOI: 10.1039/C7DT01708A.

7 M. A. Continentino, J. C. Fernandes, H. A. Borges, A. Sulpice, J.-L. Tholence, J. L. Siqueira, J. B. M. da Cunha and C. A. dos Santos, Magnetic interactions in the monoclinic ludwigite Cu2FeO2BO3, *Eur. Phys. J. B*, 1999, **9**, 613–618, DOI: 10.1007/s10051005080.

8 J. Schaefer and K. Bluhm, Zur Kristallstruktur von Cu2 M(BO3)O2 (M=Fe3+, Ga3+), *Z. Anorg. Allg. Chem.*, 1995, **621**, 571–575, DOI: 10.1002/zaac.19956210414.

9 J. P. Attfield, J. F. Clarke and D. A. Perkins, Magnetic and crystal structures of iron borates, *Phys. B*, 1992, **180**, 581–584, DOI: 10.1016/0921-4526(92)90401-D.

10 Q. Ping, B. Xu, X. Ma, J. Tian and B. Wang, An iron oxyborate Fe 3 BO 5 material as a high-performance anode for lithium-ion and sodium-ion batteries, *Dalton Trans.*, 2019, **48**(17), 5741–5748, DOI: 10.1039/C9DT00010K.

11 S. N. Sofronova, N. V. Kazak, E. V. Eremin, E. M. Moshkina, A. V. Chernyshov and A. F. Bovina, Magnetization reversal and sign reversal exchange bias field in polycrystalline Ni5.33Ta0.67B2O10, *J. Alloys Compd.*, 2021, **864**, 158200, DOI: 10.1016/j.jallcom.2020.158200.

12 S. N. Sofronova, L. N. Bezmaternykh, E. V. Eremin, I. I. Nazarenko, N. V. Volkov, A. V. Kartashev and E. M. Moshkina, The superexchange interactions and magnetic ordering in low-dimentional ludwigite Ni5GeB2O10, *J. Magn. Magn. Mater.*, 2026, **401**, 217–222, DOI: 10.1016/j.jmmm.2015.10.024.

13 E. Moshkina, S. Sofronova, A. Veligzhanin, M. Molokeev, I. Nazarenko, E. Eremin and L. Bezmaternykh, Magnetism and structure of Ni2MnBO5 ludwigite, *J. Magn. Magn. Mater.*, 2016, **402**, 69–75, DOI: 10.1016/j.jmmm.2015.11.033.

14 N. B. Ivanova, A. D. Vasil'ev, D. A. Velikanov, N. V. Kazak, S. G. Ovchinnikov, G. A. Petrakovskiĭ and V. V. Rudenko, Magnetic and electrical properties of cobalt oxyborate

Co3BO5, *Phys. Solid State*, 2007, **49**, 651–653, DOI: 10.1134/S1063783407040087.

15 D. C. Freitas, M. A. Continentino, R. B. Guimaraes, J. C. Fernandes, J. Ellena and L. Ghivelder, Structure and magnetism of homometallic ludwigites: Co3O2BO3 versus Fe3O2BO3, *Phys. Rev. B: Condens. Matter Mater. Phys.*, 2008, **77**, 184422, DOI: 10.1103/PhysRevB.77.184422.

16 M. Matos, J. Terra and D. E. Ellis, First principles calculations on the magnetic state of the mixed valence cobalt ludwigite, arXiv preprint arXiv:1802.10063, 2018. arXiv:1802.10063 [cond-mat.mtrl-sci].

17 Y. V. Knyazev, N. V. Kazak, I. I. Nazarenko, S. N. Sofronova, N. D. Rostovtsev, J. Bartolomé, A. Arauzo and S. G. Ovchinnikov, Effect of magnetic frustrations on magnetism of the Fe3BO5 and Co3BO5 ludwigites, *J. Magn. Magn. Mater.*, 2019, **474**, 493–500, DOI: 10.1016/j.jmmm.2018.10.126.

18 D. C. Freitas, C. P. C. Medrano, D. R. Sanchez, M. Nunez Regueiro, J. A. Rodríguez-Velamazán and M. A. Continentino, Magnetism and charge order in the ladder compound Co3O2BO3, *Phys. Rev. B*, 2016, **94**, 174409, DOI: 10.1103/PhysRevB.94.174409.

19 J. Bartolomé, A. Arauzo, N. V. Kazak, N. B. Ivanova, S. G. Ovchinnikov, Y. V. Knyazev and I. S. Lyubutin, Uniaxial magnetic anisotropy in Co2.25Fe0.75O2BO3 compared to Co3O2BO3 and Fe3O2BO3 ludwigites, *Phys. Rev. B: Condens. Matter Mater. Phys.*, 2011, **83**, 144426, DOI: 10.1103/PhysRevB.83.144426.

20 N. V. Kazak, M. S. Platunov, Y. V. Knyazev, M. S. Molokeev, M. V. Gorev, S. G. Ovchinnikov, Z. V. Pchelkina, V. V. Gapontsev, S. V. Streltsov, J. Bartolomé, A. Arauzo, V. V. Yumashev, S. Y. Gavrilkin, F. Wilhelm and A. Rogalev, Spin state crossover in Co3BO5, *Phys. Rev. B*, 2021, **103**, 094445, DOI: 10.1103/PhysRevB.103.094445.

21 C. W. Galdino, D. C. Freitas, C. P. C. Medrano, R. Tartaglia, D. Rigitano, J. F. Oliveira, A. A. Mendonça, *et al.*, Magnetic, electronic, structural, and thermal properties of the Co3O2BO3 ludwigite in the paramagnetic state, *Phys. Rev. B*, 2019, **100**, 165138, DOI: 10.1103/PhysRevB.100.165138.

22 D. C. Freitas, M. A. Continentino, R. B. Guimaraes, J. C. Fernandes, E. P. Oliveira, R. E. Santelli, J. Ellena, G. G. Eslava and L. Ghivelder, Partial magnetic ordering and crystal structure of the ludwigites Co2FeO2BO3 and Ni2FeO2BO3, *Phys. Rev. B: Condens. Matter Mater. Phys.*, 2009, **79**, 134437, DOI: 10.1103/PhysRevB.79.134437.

23 N. V. Kazak, N. B. Ivanova, O. A. Bayukov, S. G. Ovchinnikov, A. D. Vasiliev, V. V. Rudenko, J. Bartolomé, A. Arauzo and Y. V. Knyazev, The superexchange interactions in mixed Co–Fe ludwigite, *J. Magn. Magn. Mater.*, 2011, **323**, 521–527, DOI: 10.1016/j.jmmm.2010.09.057.

24 N. B. Ivanova, N. V. Kazak, Y. V. Knyazev, D. A. Velikanov, L. N. Bezmaternykh, S. G. Ovchinnikov, A. D. Vasiliev, M. S. Platunov, J. Bartolomé and G. S. Patrin, Crystal structure and magnetic anisotropy of ludwigite Co2FeO2BO3, *J. Exp. Theor. Phys.*, 2011, **113**, 1015–1024, DOI: 10.1134/S1063776111140172.

25 N. V. Kazak, N. B. Ivanova, V. V. Rudenko, S. G. Ovchinnikov, A. D. Vasil'ev and Y. V. Knyazev, Conductivity study of Co3O2BO3 and Co3-xFexO2BO3 oxyborates, *Solid State Phenomena*, 2009, **152**, 104–107, DOI: 10.4028/www.scientific.net/SSP.152-153.104.

26 E. C. Dos Santos, D. C. Freitas, I. Fier, J. C. Fernandes, M. A. Continentino, A. J. A. De Oliveira and L. Walmsley, Current controlled negative differential resistance behavior in Co2FeO2BO3 and Fe3O2BO3 single crystals, *J. Phys. Chem. Solids*, 2016, **90**, 65–68, DOI: 10.1016/j.jpcs.2015.11.015.

27 J. P. Perdew, K. Burke and M. Ernzerhof, Generalized gradient approximation made simple, *Phys. Rev. Lett.*, 1996, **77**, 3865–3868; J. P. Perdew, K. Burke and M. Ernzerhof, Errata: Generalized gradient approximation made simple, *Phys. Rev. Lett.*, 1997, **78**, 1396, DOI: 10.1103/PhysRevLett.77.3865.

28 G. Kresse and J. Furthmuller, Efficiency of ab initio total energy calculations for metals and semiconductors using a plane-wave basis set, *Comput. Mater. Sci.*, 1996, **6**, 15–50; G. Kresse and J. Furthmuller, Efficient iterative schemes for ab initio totalenergy calculations using a plane-wave basis set, *Phys. Rev. B: Condens. Matter Mater. Phys.*, 1996, **54**, 11169–11186, DOI: 10.1103/PhysRevB.54.11169.

29 H. J. Monkhorst and J. D. Pack, Special points for Brillouinzone integrations, *Phys. Rev. B: Solid State*, 1976, **13**, 5188–5192, DOI: 10.1103/PhysRevB.13.5188.

30 H. M. Petrilli, P. E. Blöchl, P. Blaha and K. Schwarz, Electric-field-gradient calculations using the projector augmented wave method, *Phys. Rev. B: Condens. Matter Mater. Phys.*, 1998, **57**, 14690, DOI: 10.1103/PhysRevB.57.14690.

31 J. Sun, A. Ruzsinszky and J. P. Perdew, Strongly Constrained and Appropriately Normed Semilocal Density Functional, *Phys. Rev. Lett.*, 2015, **115**, 036402, DOI: 10.1103/PhysRevLett.115.036402.

32 A. P. Douvalis, A. Moukarika, T. Bakas, G. Kallias and V. Papaefthymiou, Mössbauer and magnetization studies of Fe3BO5, *J. Phys.: Condens. Matter*, 2002, **14**, 3303, DOI: 10.1088/0953-8984/14/12/317.

33 J. Larrea, D. R. Sanchez, F. J. Litterst, E. M. Baggio-Saitovitch, J. C. Fernandes, R. B. Guimaraes and M. A. Continentino, Magnetism and charge ordering in Fe3O2BO3 studied by 57 Fe Mössbauer spectroscopy, *Phys. Rev. B: Condens. Matter Mater. Phys.*, 2004, **70**, 174452, DOI: 10.1103/PhysRevB.70.174452.

34 J. C. Fernandes, R. B. Guimaraes, M. A. Continentino, H. A. Borges, A. Sulpice, J. L. Tholence, J. L. Siqueira, L. I. Zawislak, J. B. M. Da Cunha and C. A. Dos Santos, Magnetic interactions in the ludwigite Ni2FeO2BO3, *Phys. Rev. B: Condens. Matter Mater. Phys.*, 1998, **58**, 287, DOI: 10.1103/PhysRevB.58.287.

35 A. Wiedenmann, P. Burlet and R. Chevalier, Mössbauer study of imperfect one dimensional magnetic systems

FeMgBO4 and FeMg2BO5, *J. Magn. Magn. Mater.*, 1980, **15**, 216–218, DOI: 10.1016/0304-8853(80)91021-5.

36 M. Eibschütz, L. Pfeiffer and J. W. Nielsen, Critical–Point Behavior of FeBO3 Single Crystals by Mössbauer Effect, *J. Appl. Phys.*, 1970, **41**, 1276–1277, DOI: 10.1063/1.1658911.

37 Y. V. Knyazev, N. B. Ivanova, O. A. Bayukov, N. V. Kazak, L. N. Bezmaternykh and A. D. Vasiliev, Evolution of the Mössbauer spectra of ludwigite Co3–xFexO2BO3 with substitution of iron for cobalt, *Phys. Solid State*, 2013, **55**, 1175–1179, DOI: 10.1134/S1063783413060176.

38 G. A. Petrakovskiĭ, L. N. Bezmaternykh, D. A. Velikanov, A. M. Vorotynov, O. A. Bayukov and M. Schneider, Magnetic properties of single crystals of ludwigites Cu2MBO5 (M=Fe3+, Ga3+), *Phys. Solid State*, 2009, **51**, 2077–2083, DOI: 10.1134/S106378340910014X.

39 D. A. Perkins and J. P. Attfield, Resonant powder X-ray determination of the cation distribution in FeNi2BO5, *J. Chem. Soc., Chem. Commun.*, 1991, **4**, 229–231, DOI: 10.1039/C39910000229.

40 R. D. Shannon, Revised effective ionic radii and systematic studies of interatomic distances in halides and chalcogenides, *Acta Crystallogr., Sect. A: Cryst. Phys., Diffr., Theor. Gen. Crystallogr.*, 1976, **32**, 751–767, DOI: 10.1107/S0567739476001551.